

Supplement of Biogeosciences, 12, 4621–4635, 2015  
<http://www.biogeosciences.net/12/4621/2015/>  
doi:10.5194/bg-12-4621-2015-supplement  
© Author(s) 2015. CC Attribution 3.0 License.



*Supplement of*

## **Deriving seasonal dynamics in ecosystem properties of semi-arid savanna grasslands from in situ-based hyperspectral reflectance**

**T. Tagesson et al.**

*Correspondence to:* T. Tagesson (torbern.tagesson@ign.ku.dk)

The copyright of individual parts of the supplement might differ from the CC-BY 3.0 licence.

## S1. Seasonal dynamics in effects of varying sun and sensor viewing geometry on NDSI

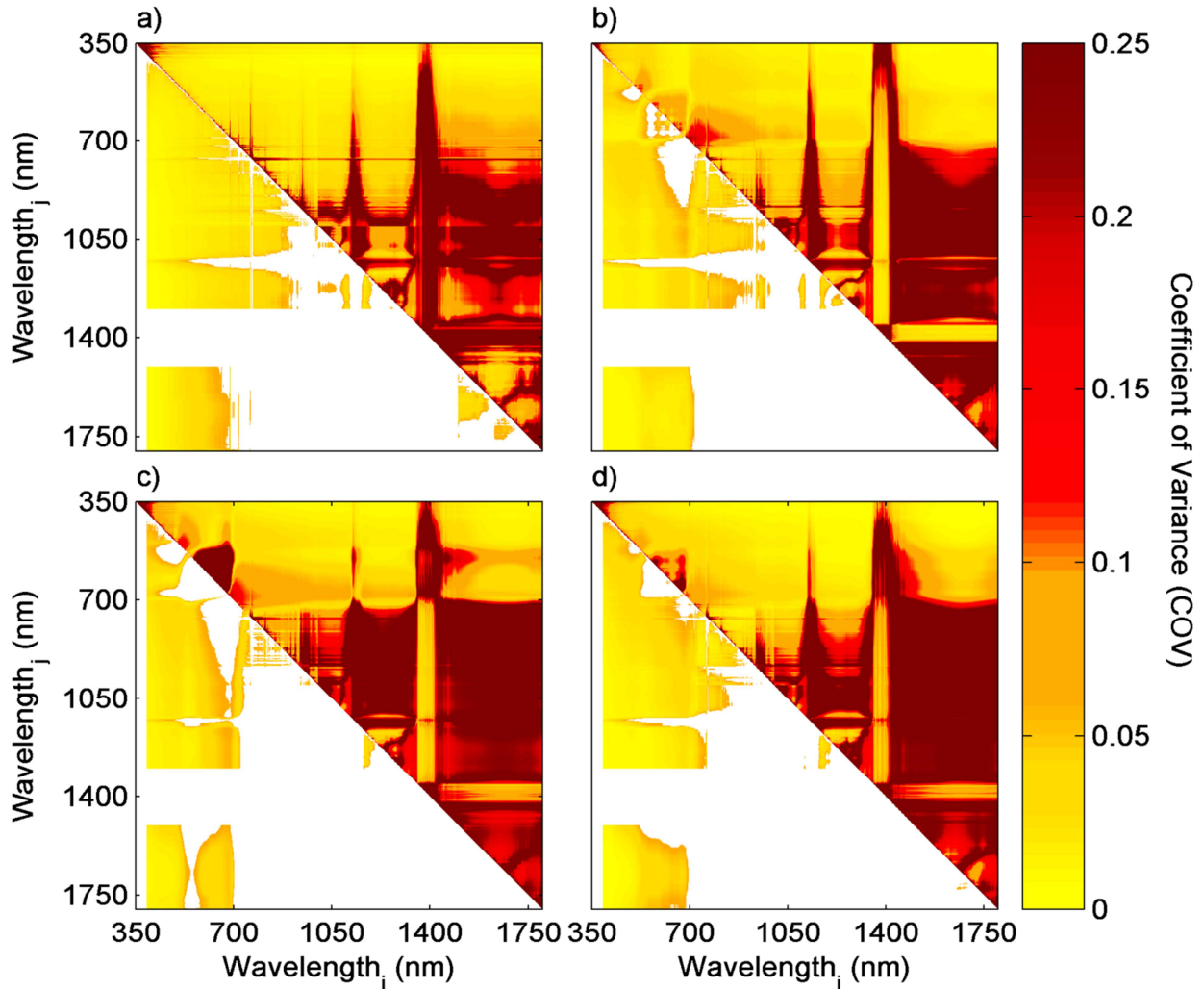


Figure S1. The coefficient of variation (COV), i.e. the ratio between daily standard deviation and the daily mean (measurements taken between 8:00 and 18:00 (UTC)), for different normalised difference spectral index (NDSI) wavelength ( $i, j$ ) combinations for: a) 10 days during the dry season 2012 (day of year 71-85;  $n=480$ ), b) 11 days during the grow-up phase in 2011 (day of year 200-214;  $n=528$ ), c) 12 days at the peak of the growing season 2011 (day of year 237-251;  $n=576$ ), and d) 12 days during the senescent phase 2011 (day of year 278-293;  $n=576$ ). The COV indicates how strongly the NDSI are affected by variable sun angles. The upper right half of each chart shows the unfiltered  $R^2$  values whereas the lower left half includes filtering as based on criteria described under Subsect. 2.6.

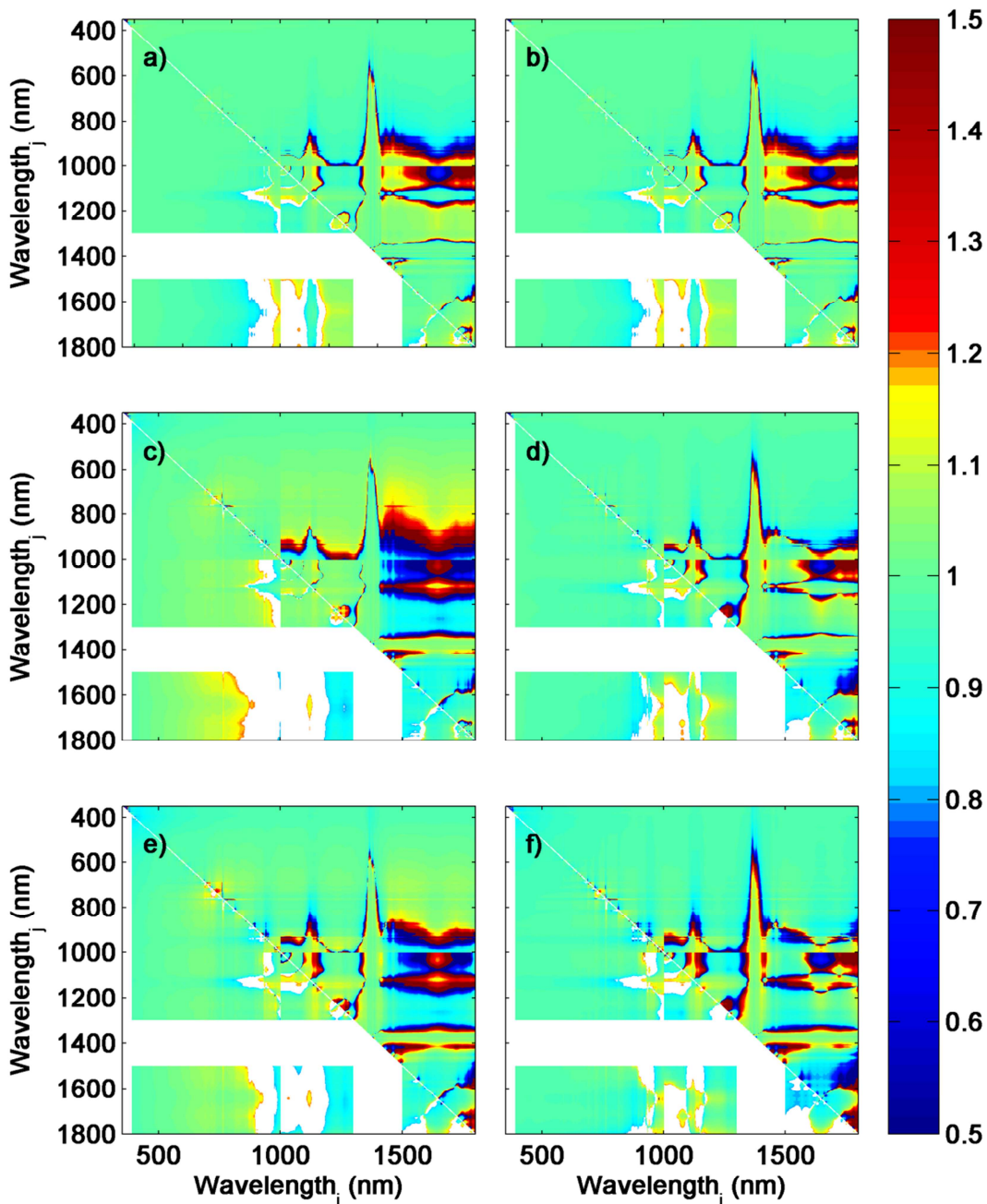


Figure S2. The anisotropy factor (ANIF) for different normalised difference spectral index (NDSI) wavelength ( $i, j$ ) combinations for 10 days during the dry season 2012 (day of year 71-85) for the different sensor viewing angles: a)  $15^\circ\text{E}$ , b)  $15^\circ\text{W}$ , c)  $30^\circ\text{E}$ , d)  $30^\circ\text{W}$ , e)  $45^\circ\text{E}$ , and f)  $45^\circ\text{W}$ . In order not to include effects of solar zenith angles in the analysis, only data measured between 12:00 and 14:00 (UTC) were used in the ANIF calculations ( $n=90$ ). The upper right half of each chart shows the unfiltered  $R^2$  values whereas the lower left half includes filtering as based on criteria described under Subsect. 2.6.

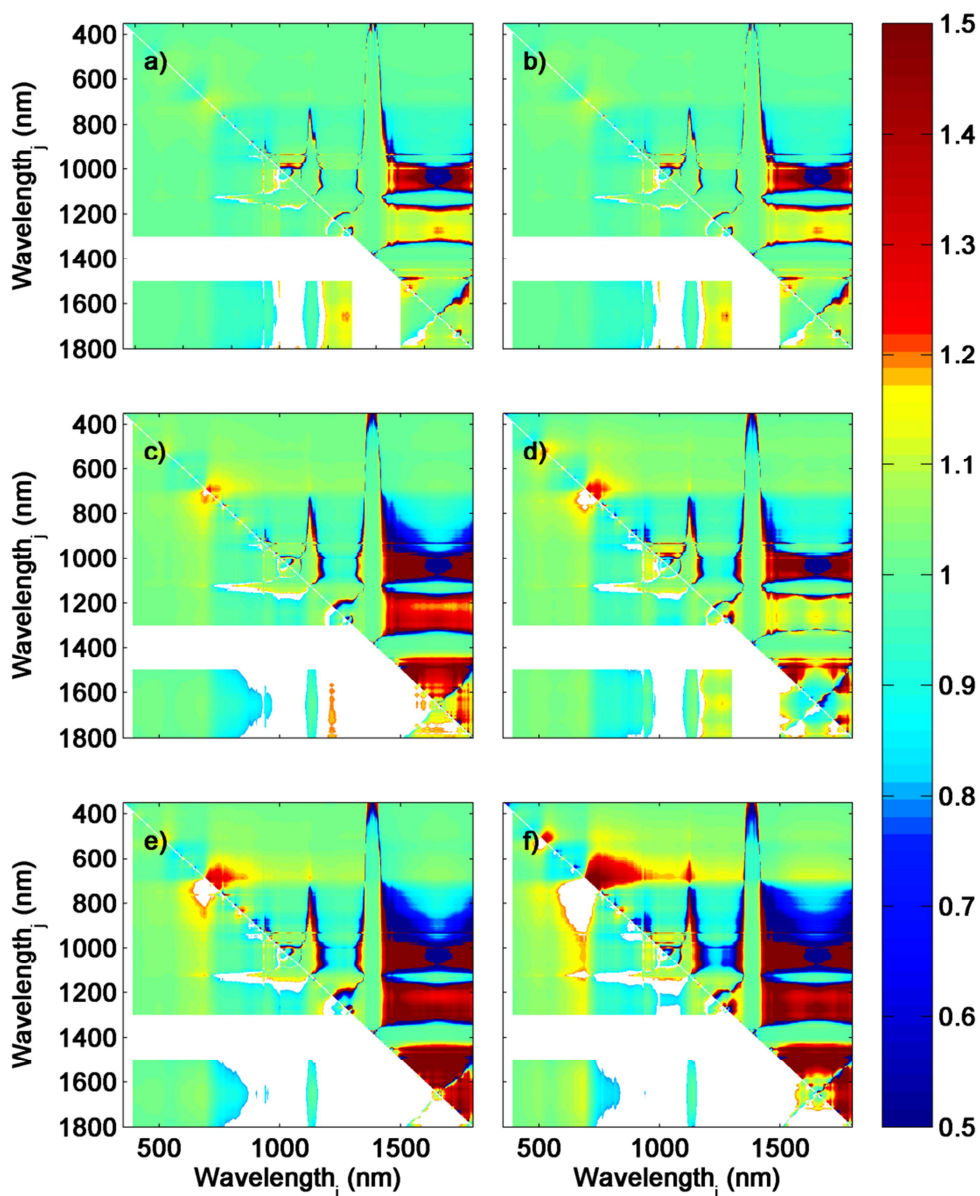


Figure S3. The anisotropy factor (ANIF) for different normalised difference spectral index (NDSI) wavelength ( $i, j$ ) combinations for 11 days during the fast growth period (period of vegetation establishment) in 2011 (day of year 200-214) for the different sensor viewing angles: a)  $15^\circ\text{E}$ , b)  $15^\circ\text{W}$ , c)  $30^\circ\text{E}$ , d)  $30^\circ\text{W}$ , e)  $45^\circ\text{E}$ , and f)  $45^\circ\text{W}$ . In order not to include effects of solar zenith angles in the analysis, only data measured between 12:00 and 14:00 (UTC) were used in the ANIF calculations ( $n=99$ ). The upper right half of each chart shows the unfiltered  $R^2$  values whereas the lower left half includes filtering as based on criteria described under Subsect. 2.6.

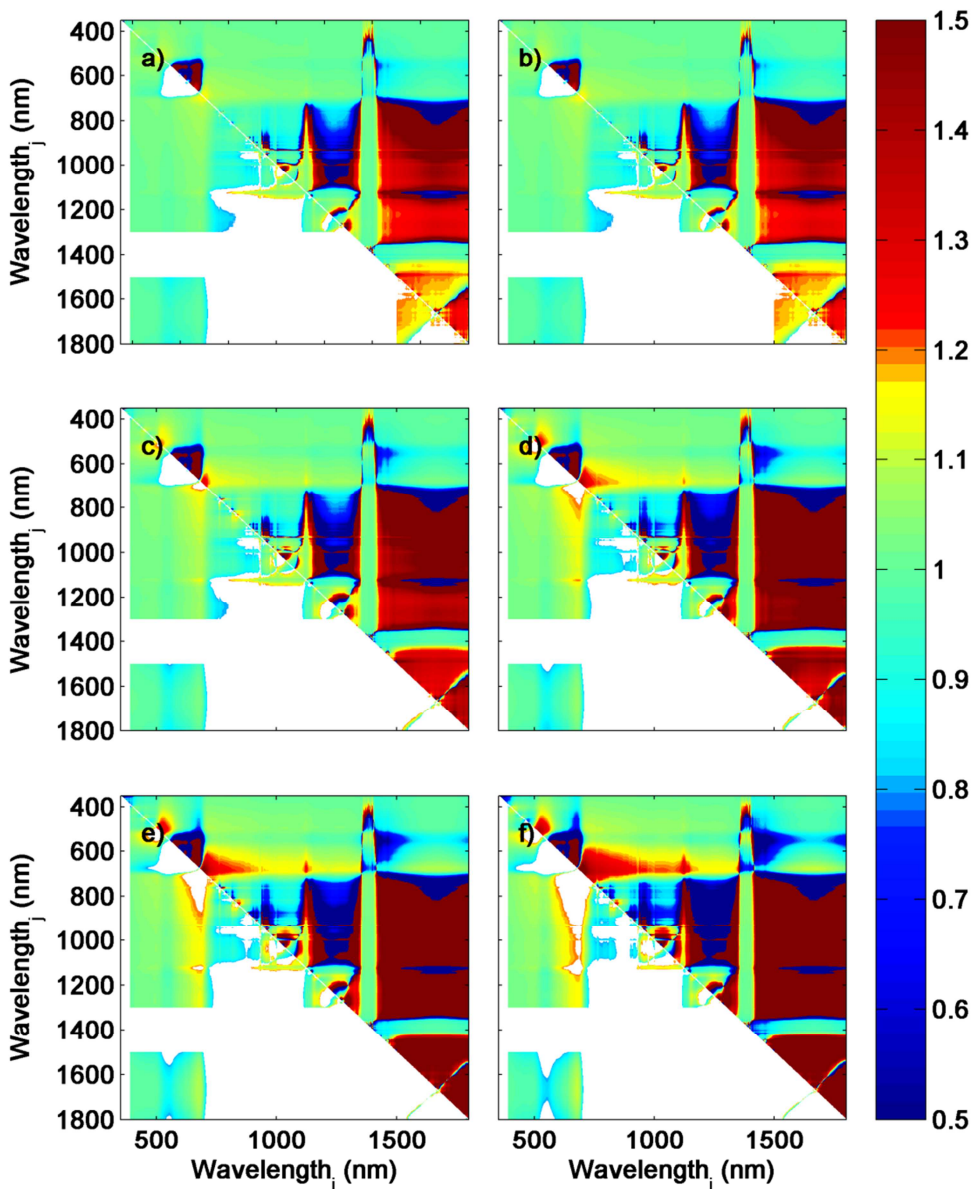


Figure S4. The anisotropy factor (ANIF) for different normalised difference spectral index (NDSI) wavelength ( $i, j$ ) combinations for 12 days at the peak of the growing season 2011 (day of year 237-251) for the different sensor viewing angles: a)  $15^\circ\text{E}$ , b)  $15^\circ\text{W}$ , c)  $30^\circ\text{E}$ , d)  $30^\circ\text{W}$ , e)  $45^\circ\text{E}$ , and f)  $45^\circ\text{W}$ . In order not to include effects of solar zenith angles in the analysis, only data measured between 12:00 and 14:00 (UTC) were used in the ANIF calculations ( $n=108$ ). The upper right half of each chart shows the unfiltered  $R^2$  values whereas the lower left half includes filtering as based on criteria described under Subsect. 2.6.

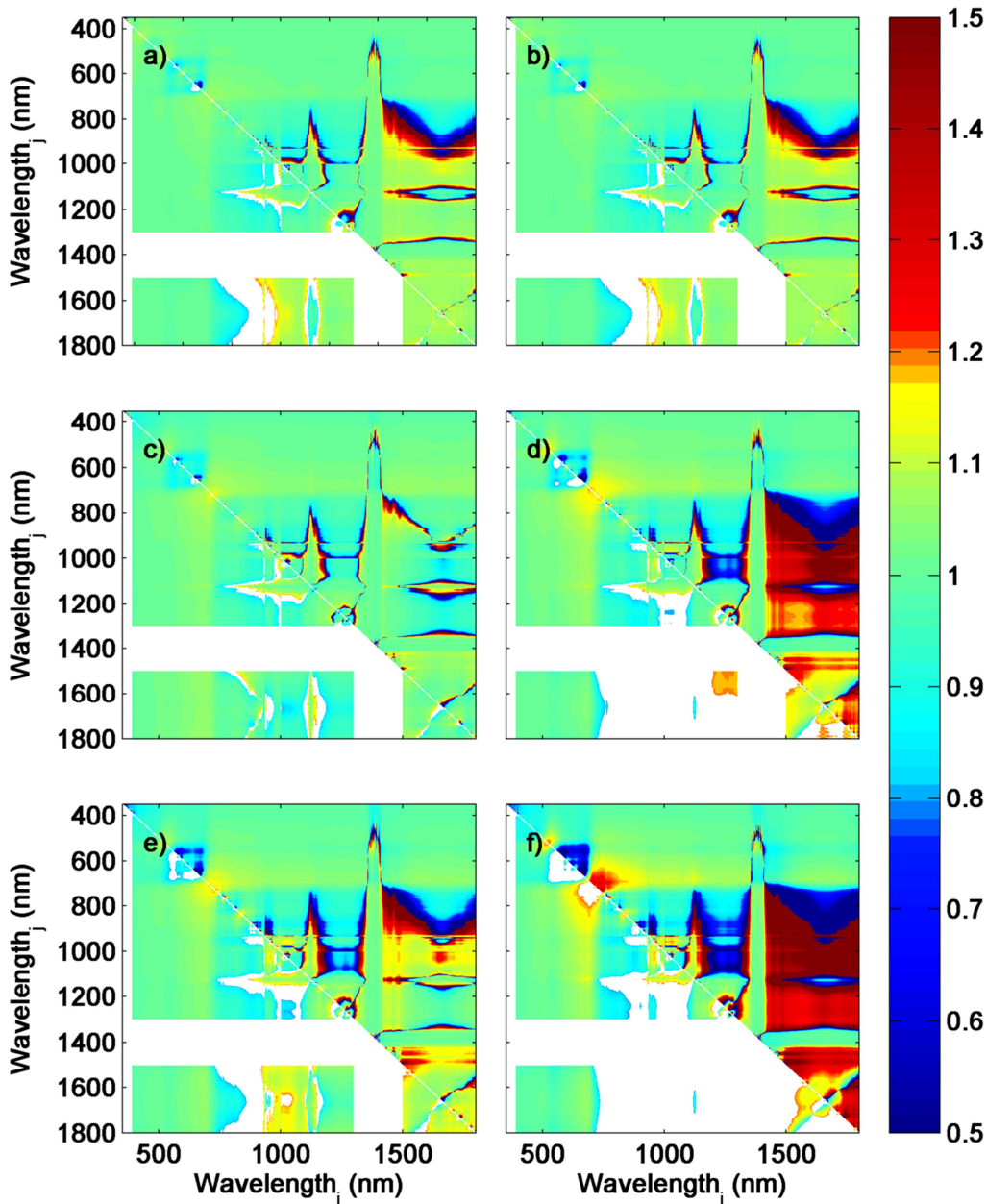


Figure S5. The anisotropy factor (ANIF) for different normalised difference spectral index (NDSI) wavelength ( $i, j$ ) combinations for 12 days at the end of the growing season 2011 (day of year 278-293) for the different sensor viewing angles: a)  $15^\circ\text{E}$ , b)  $15^\circ\text{W}$ , c)  $30^\circ\text{E}$ , d)  $30^\circ\text{W}$ , e)  $45^\circ\text{E}$ , and f)  $45^\circ\text{W}$ . In order not to include effects of solar zenith angles in the analysis, only data measured between 12:00 and 14:00 (UTC) were used in the ANIF calculations ( $n=108$ ). The upper right half of each chart shows the unfiltered  $R^2$  values whereas the lower left half includes filtering as based on criteria described under Subsect. 2.6. The pronounced difference in the E and W direction during the senescent phase is most likely caused by heterogeneity in vegetation structure of the herbaceous vegetation caused by the wind.

## S2. Differences between linear and exponential relationships fitted between NDSI and the ecosystem properties

We examined the relationship between the normalised difference spectral indices (NDSI) from nadir observations and response variables (biomass, gross primary productivity (GPP), light use efficiency (LUE), and fraction of photosynthetically active radiation (FAPAR) using both linear and exponential regression analysis. The linear regression analysis is described in the main paper. Additionally, we fitted ordinary least square exponential regression equations between NDSI and the response variables using:

$$Y = a \times \exp^{b \times \text{NDSI}} \quad (\text{S1})$$

where Y is the response variable, and a, and b are fitted parameters.

The linear and exponential regression equations generated very similar coefficients of determination ( $R^2$ ), and the pattern of how well the different wavelengths predicted variability in seasonal dynamics of the response variables were also similar (compare Fig. S6 with Fig. 6 in the main paper). The difference in  $R^2$  between the two regression models were generally less than 0.05 (Fig. S7) and only few wavelength combinations had stronger relationships using exponential or linear models (areas coloured in dark blue and red, respectively (Fig. S7)). No significant difference was found between the two model equations.

For biomass, the strongest exponential relationship was seen at NDSI[412,1131], for which the exponential model increased the  $R^2$  from 0.88 to 0.89 in relation to the best linear model (Fig. S8). For GPP, the strongest exponential relationships was found at NDSI[933,702], but  $R^2$  decreased from 0.86 to 0.82 in relation to the strongest linear model. For LUE, the strongest exponential relationship was observed at NDSI[456,481] with an  $R^2$  of 0.83, whereas the linear model with the strongest correlation had an  $R^2$  of 0.81. For FAPAR, the strongest linear and exponential relationships were found for exactly the same wavelength combination NDSI[399,1295], but the exponential model decreased the  $R^2$  from 0.81 to 0.78.

The measurements of the experiment are conducted in a semi-arid ecosystem with relatively low vegetation density. Maximum LAI measured between 2002 and 2013 was 2.1 (Tagesson et al. 2015), hence there is limited saturation effects. In case the linear relationship is strong, it indicates minor problems with saturation. For particular wavelength regions being sensitive to saturation effects, exponential and logarithmic regressions could fit better. However, in this study the aim is to identify wavelength regions with maximum sensitivity to seasonal dynamics in ecosystem properties, and therefore wavelength regions sensitive to saturation should be avoided. Additionally, the exponential character makes the models less appropriate for upscaling applications since errors also propagate in an exponential way. In the main analysis, we have therefore chosen the usage of linear regression models.

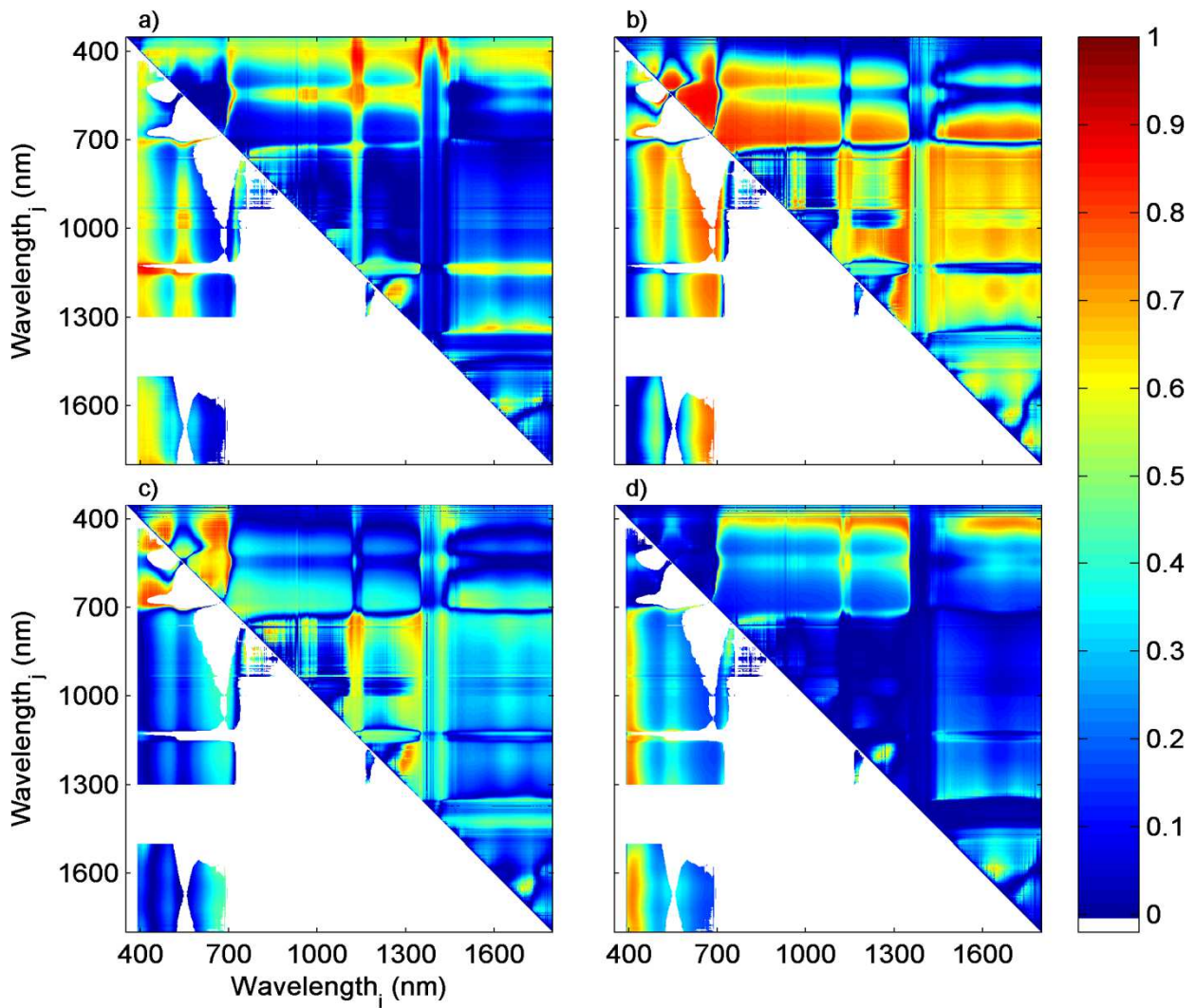


Figure S6. Coefficient of determination ( $R^2$ ) between normalised difference spectral index (NDSI) and a) dry weight biomass ( $n=12$ ;  $\text{g m}^{-2}$ ), b) gross primary productivity (GPP) ( $n=285$ ;  $\text{g C day}^{-1}$ ), c) light use efficiency (LUE) ( $n=272$ ;  $\text{g C MJ}^{-1}$ ), and d) fraction of photosynthetically active radiation absorbed by the vegetation (FAPAR) ( $n=369$ ) fitting a ordinary least square exponential regression equation. The upper right half of each chart shows the unfiltered  $R^2$  values, whereas the lower left half shows filtered  $R^2$ , based on the filtering criteria described under Subsect. 2.6.

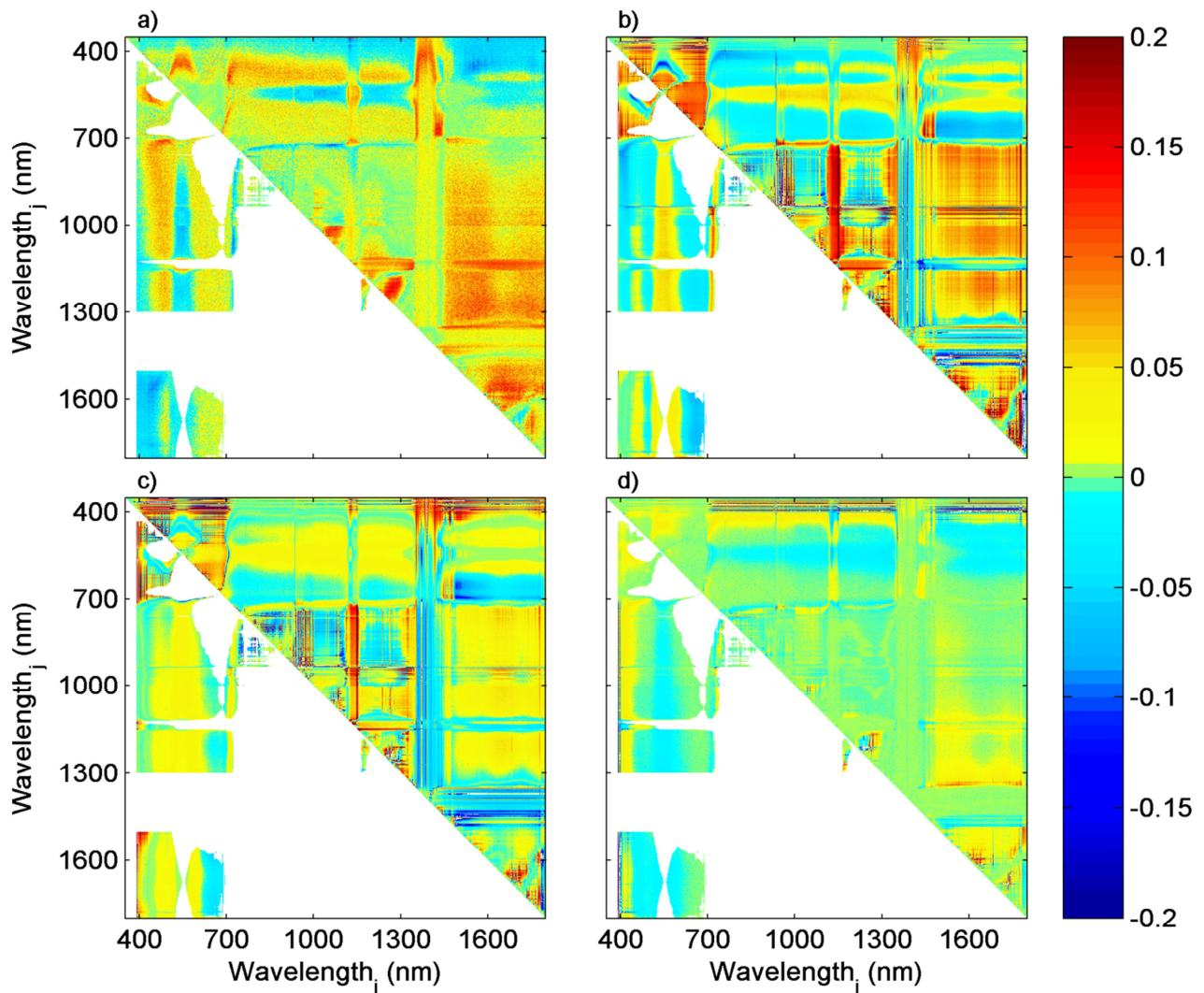


Figure S7. Difference in coefficient of determination ( $R^2$ ) between fitted linear regression equations and exponential regression equations. The equations were fitted between normalised difference spectral index (NDSI) and a) dry weight biomass ( $n=12$ ;  $\text{g m}^{-2}$ ), b) gross primary productivity (GPP) ( $n=285$ ;  $\text{g C day}^{-1}$ ), c) light use efficiency (LUE) ( $n=272$ ;  $\text{g C MJ}^{-1}$ ), and d) fraction of photosynthetically active radiation absorbed by the vegetation (FAPAR) ( $n=369$ ). The upper right half of each chart shows the unfiltered  $R^2$  values, whereas the lower left half shows filtered  $R^2$ , based on the filtering criteria described under Subsect. 2.6. Positive values indicate higher  $R^2$  for the linear regression and negative values indicate higher  $R^2$  values for the exponential regression equation.

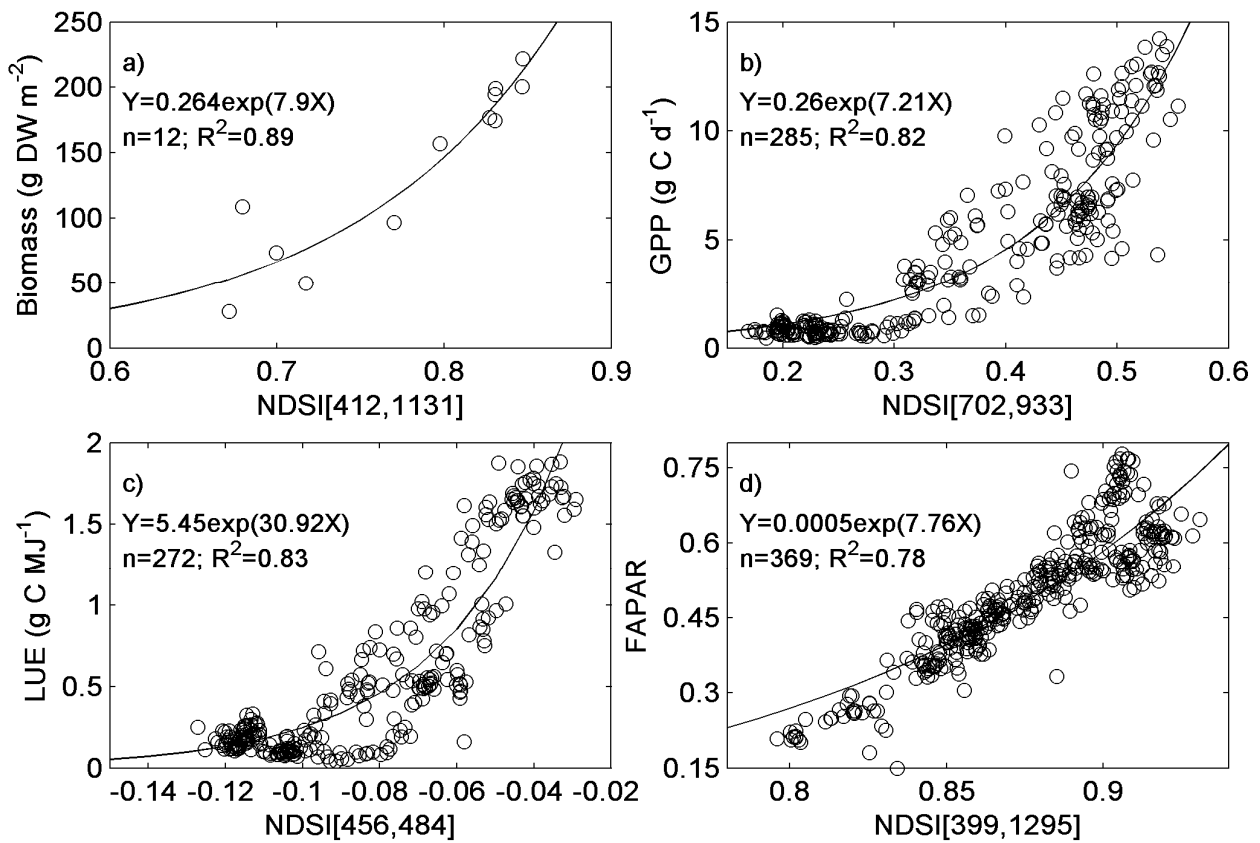


Figure S8. The least square exponential regressions with the strongest relationships between the normalised difference spectral index (NDSI) and a) dry weight biomass, b) gross primary productivity (GPP), c) light use efficiency (LUE), and d) fraction of photosynthetically active radiation absorbed by the vegetation (FAPAR).

## References

Tagesson, T., Fensholt, R., Guiro, I., Rasmussen, M.O., Huber, S., Mbow, C., Garcia, M., Horion, S., Sandholt, I., Rasmussen, B.H., Götsche, F.M., Ridler, M.-E., Olén, N., Olsen, J.L., Ehammer, A., Madsen, M., Olesen, F.S., & Ardö, J. (2015). Ecosystem properties of semi-arid savanna grassland in West Africa and its relationship to environmental variability. *Global Change Biology*, *21*, 250-264